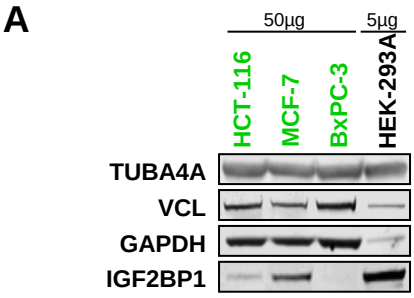

B

Correlation in the Cancer Cell Line Encyclopedia (CCLE)

	CDH1		VIM	
	Pearson R	Pearson p	Pearson R	Pearson p
IGF2BP1	-0.088	8.00E-03	0.117	3.80E-04
IGF2BP2	0.163	6.90E-07	0.159	1.30E-06
IGF2BP3	-0.059	0.07	0.138	2.90E-05
VIM	-0.606	6.80E-93	nD	nD

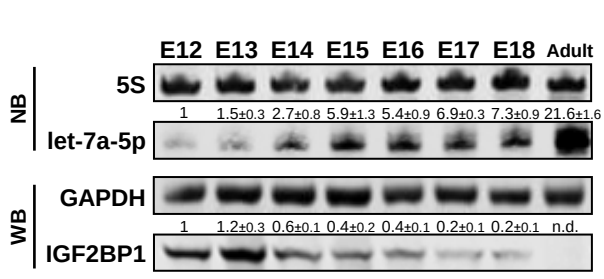

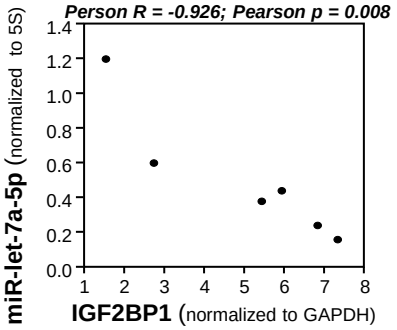

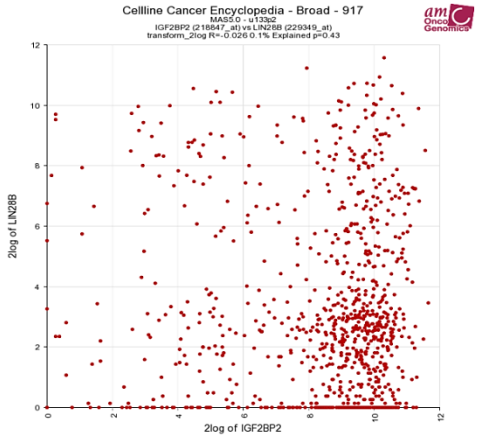

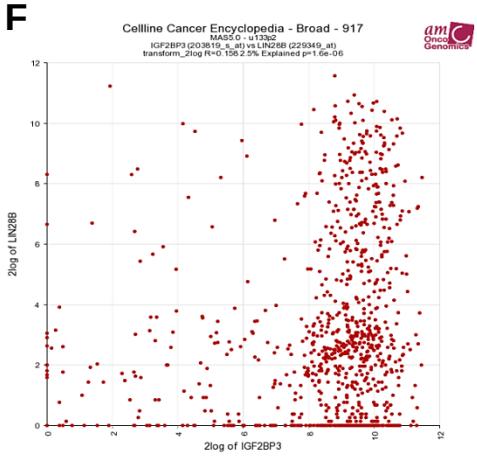

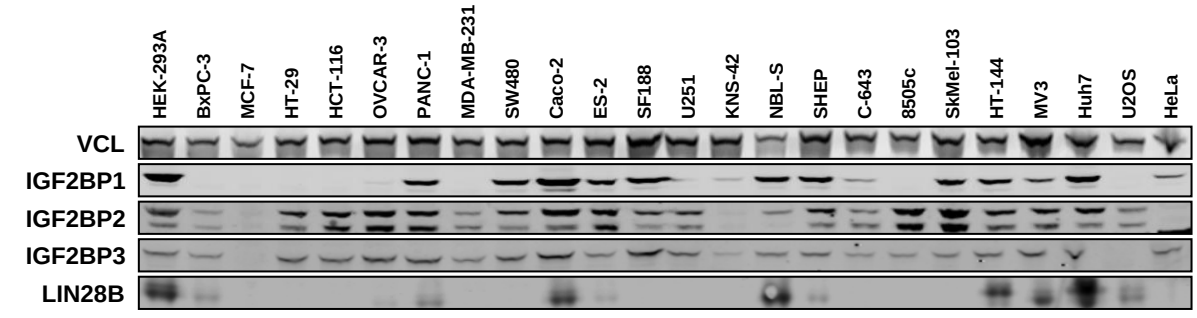

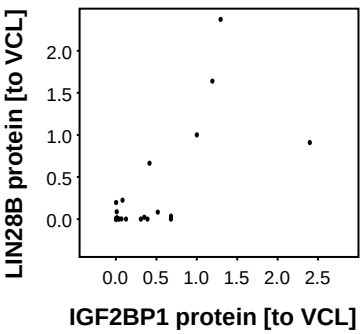

I

LIN28B (protein)		
Protein	Pearson R	Pearson p
IGF2BP1	0.698	1.49E-04
IGF2BP2	-0.034	0.876
IGF2BP3	0.292	0.166

J

IGF2BP1 (CCLE; present 347 / 917))				
Rank	Gene	Pearson R	Pearson p	present
1	LIN28B	0.317	8.20E-19	288
2	IGF2BP3	0.305	2.00E-17	854
17	HMGA2	0.255	4.60E-12	659

Supplemental Figure 1. Busch et al.

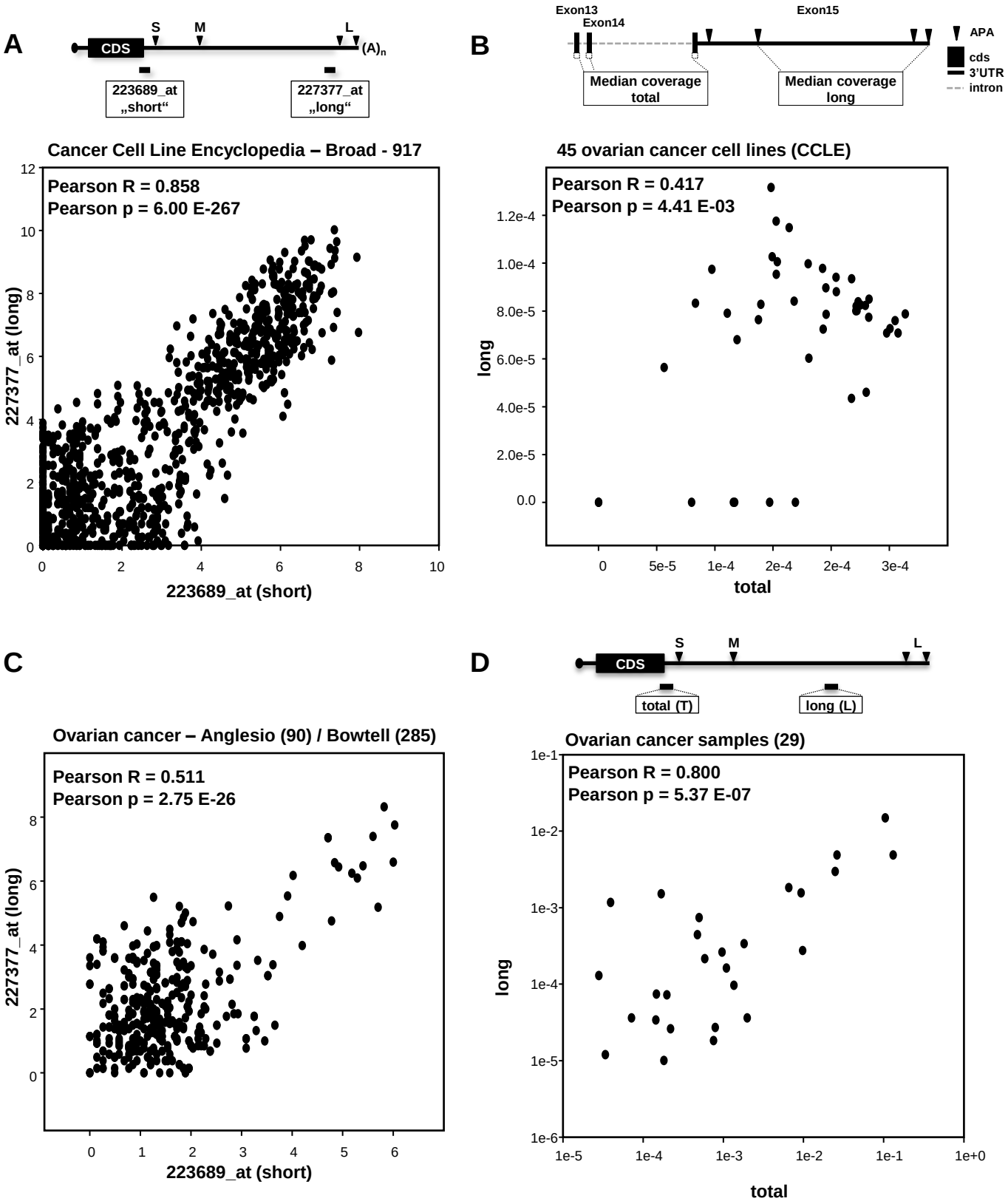

Supplemental Figure 2. Busch et al.

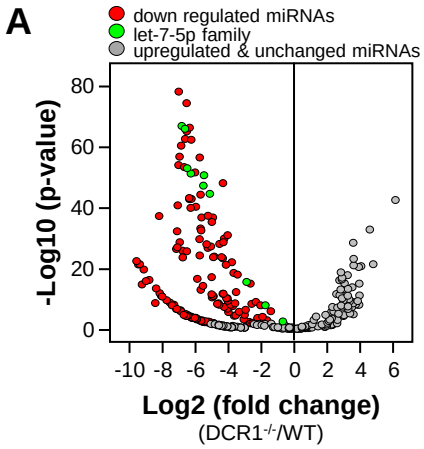

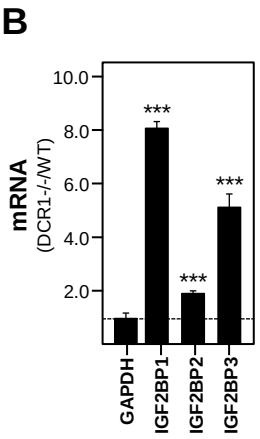

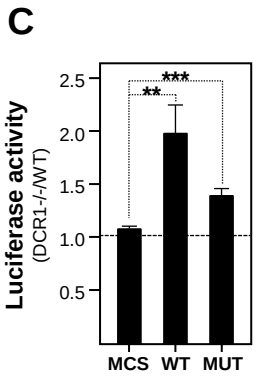

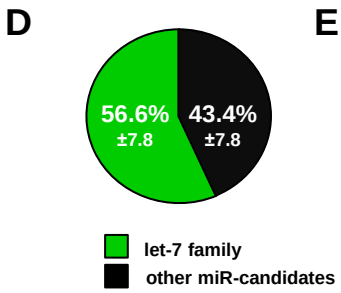

E

miRNA	targeting sites	prediction
let-7-5p family (9)	1618, 1633, 4255, 4909, 5553	Boyerinas et al. 2008
mir-17-5p family (3)	229, 1442, 4034, 5089, 5147, 5538	miRANDA
mir-196-5p family (2)	1631, 4268, 4922	Rebucci et al. 2015
mir-24-3p	1837, 2974, 4287	miRANDA
mir-181-5p family (4)	59	RNA-hybrid

Supplemental Figure 3. Busch et al.

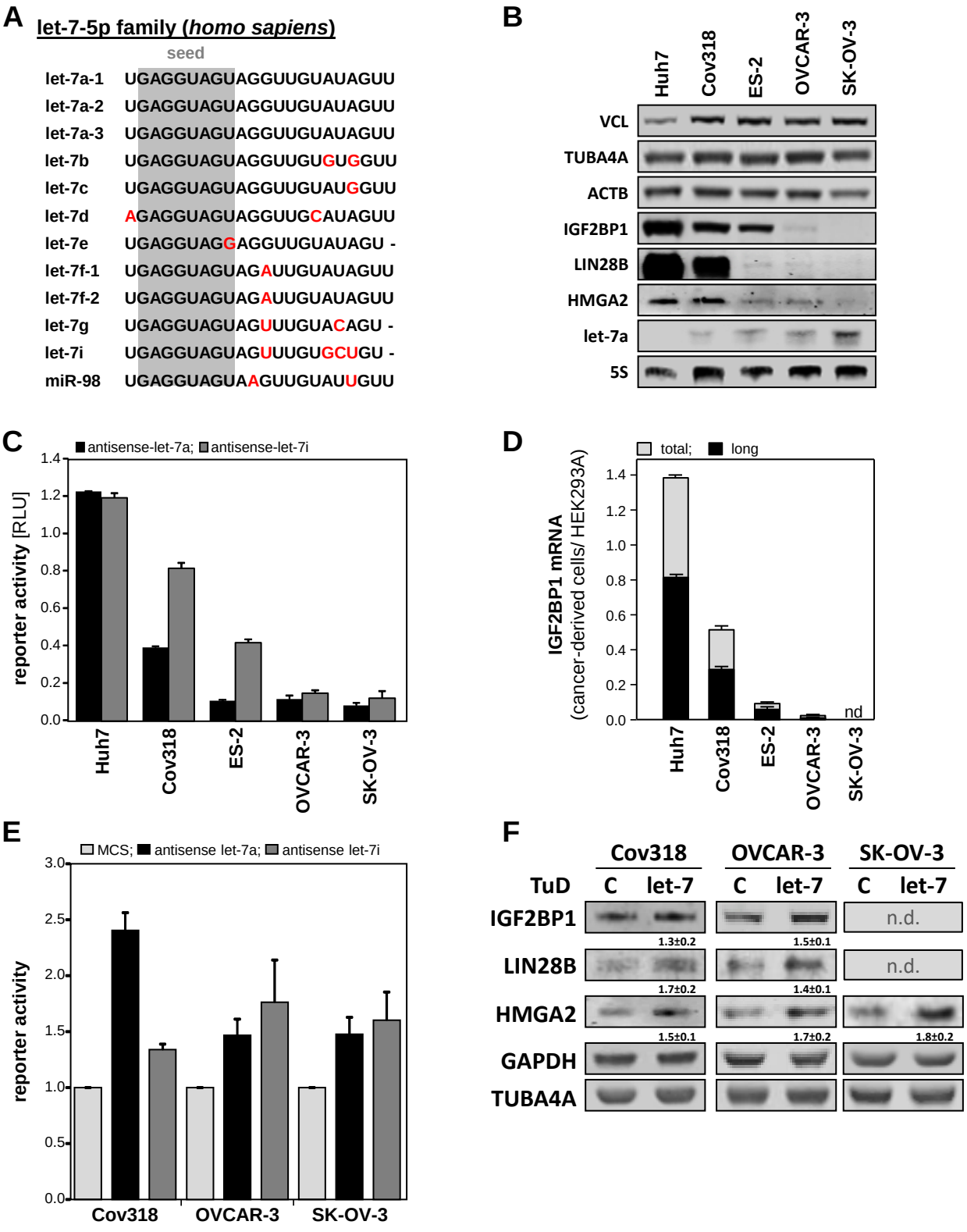

Supplemental Figure 4. Busch et al.

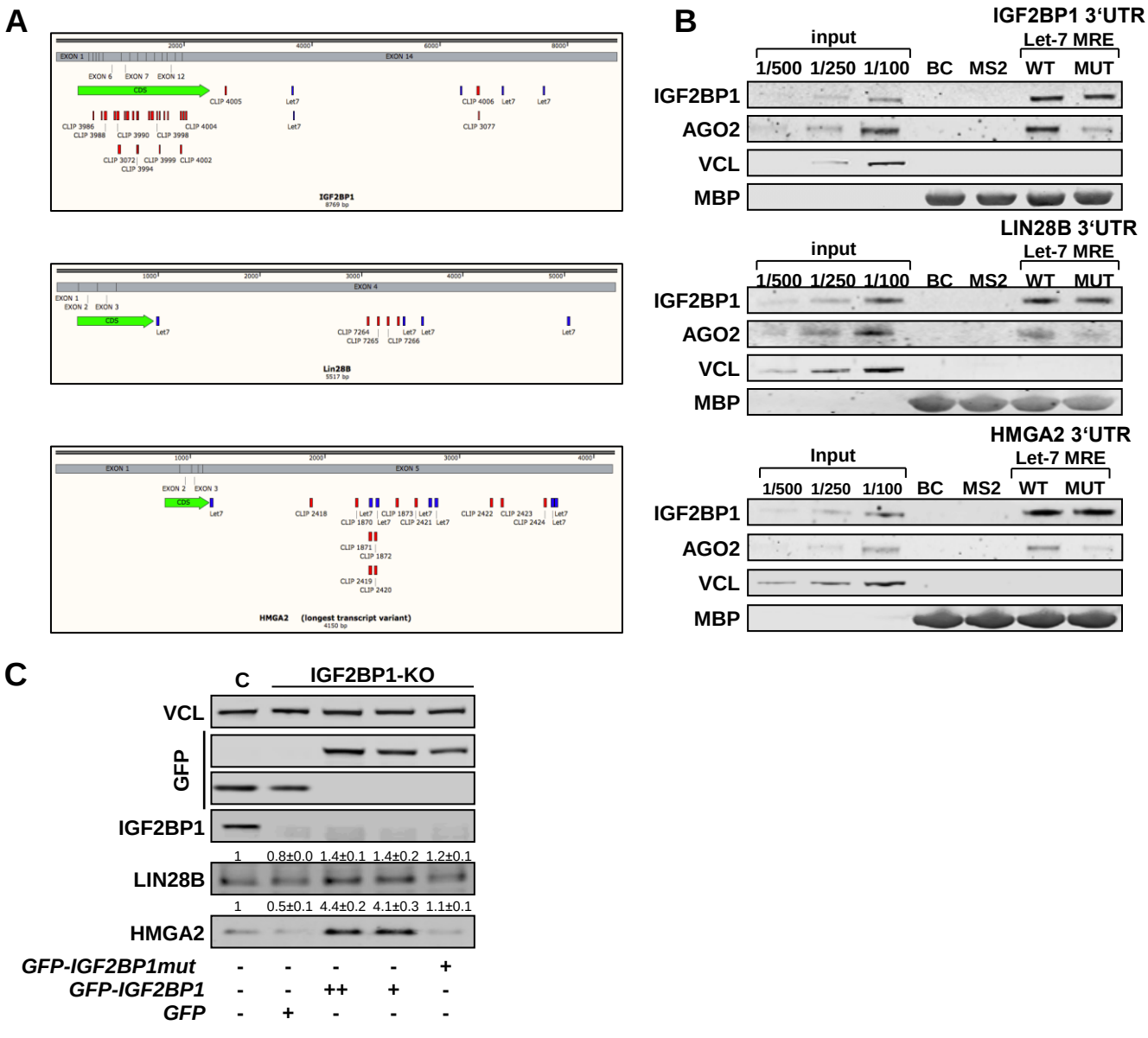

Supplemental Figure 5. Busch et al.

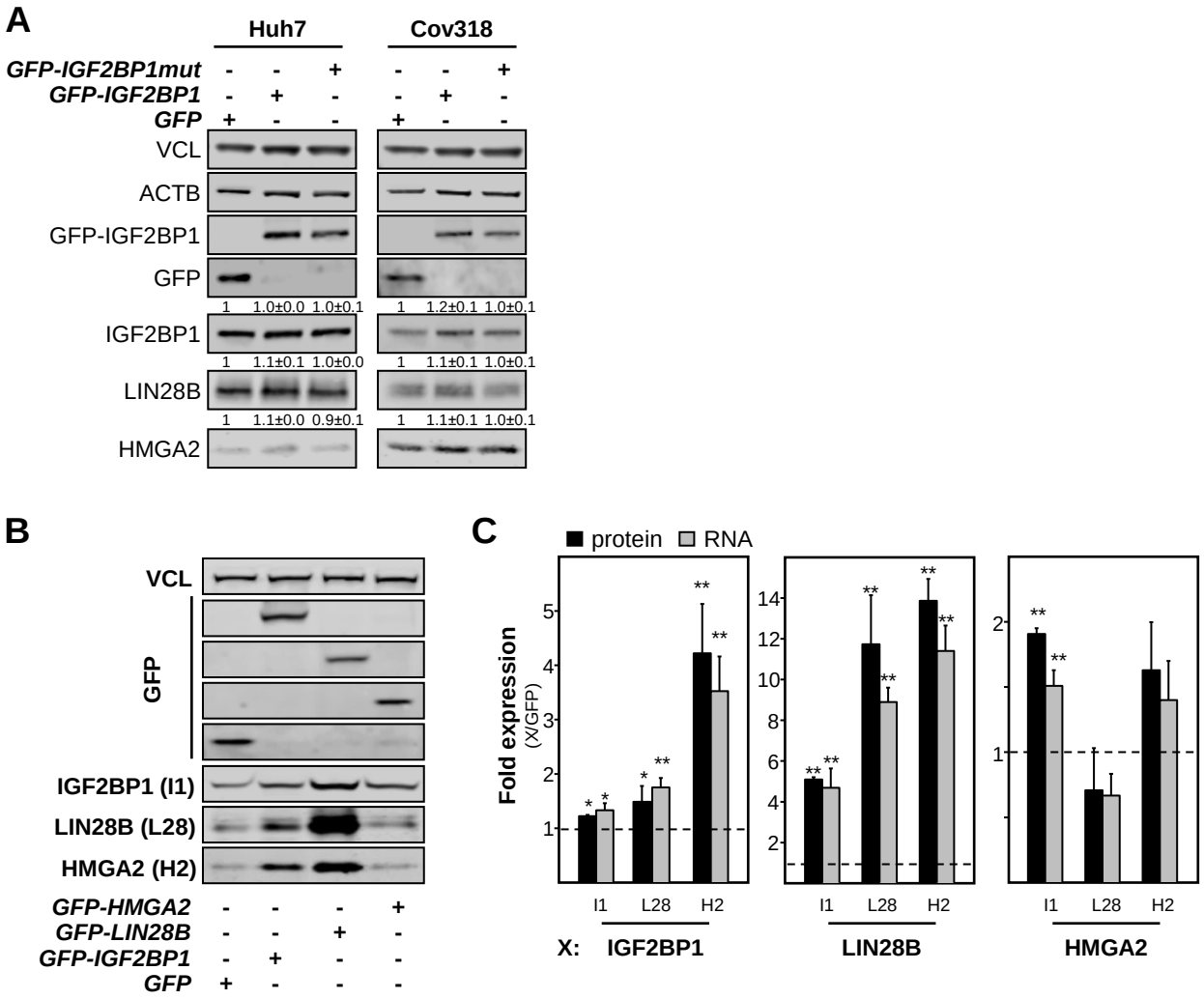

Supplemental Figure 6. Busch et al.

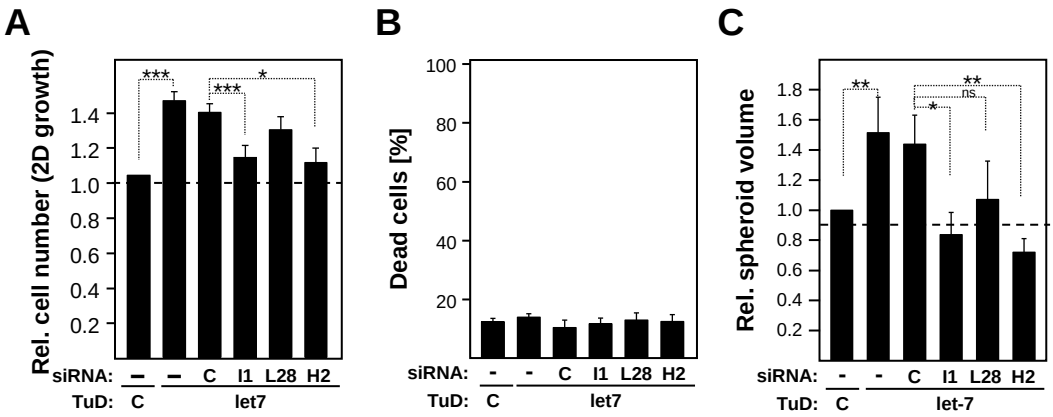

Supplemental Figure 7. Busch et al.

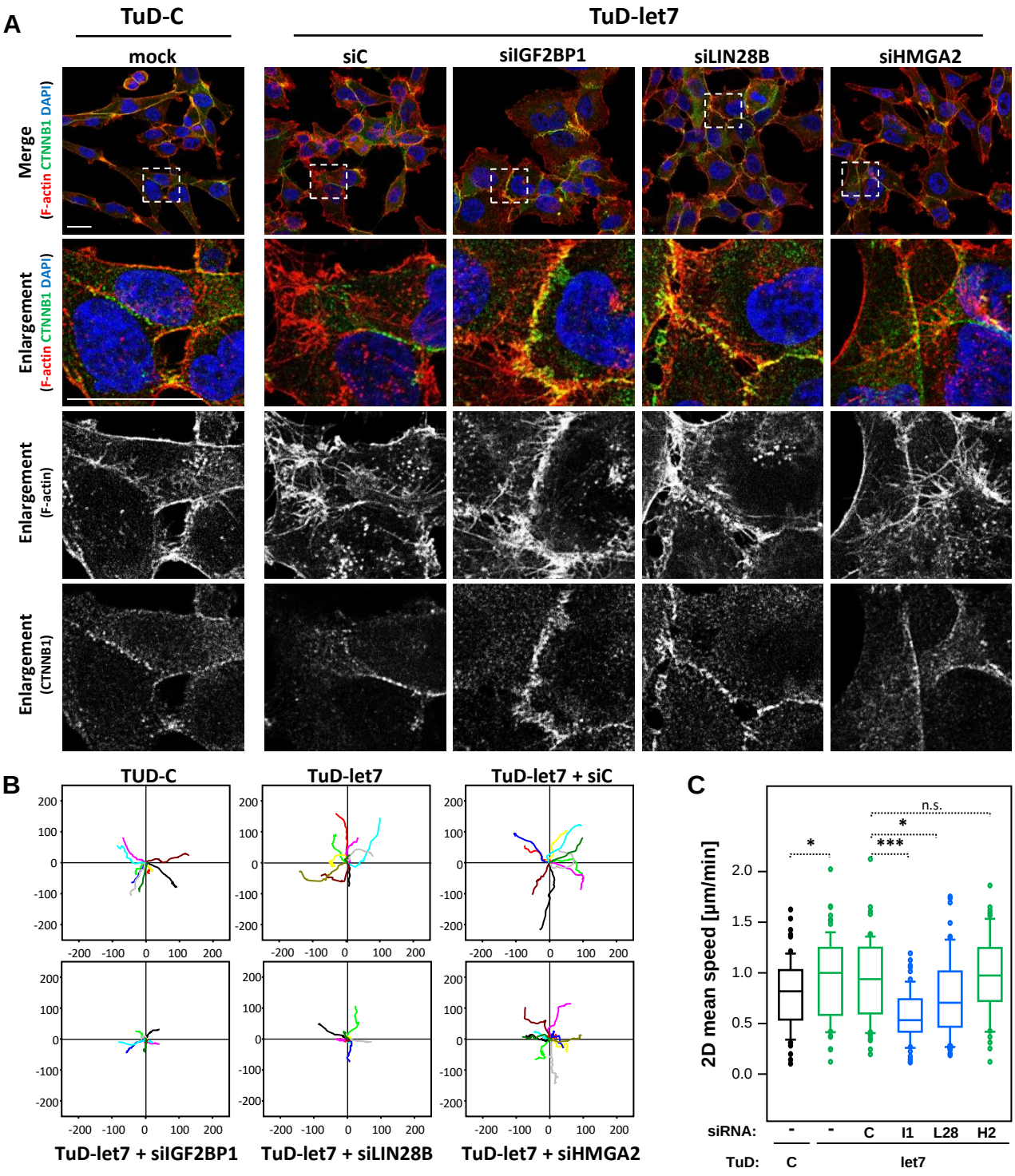

Supplemental Figure 8. Busch et al.

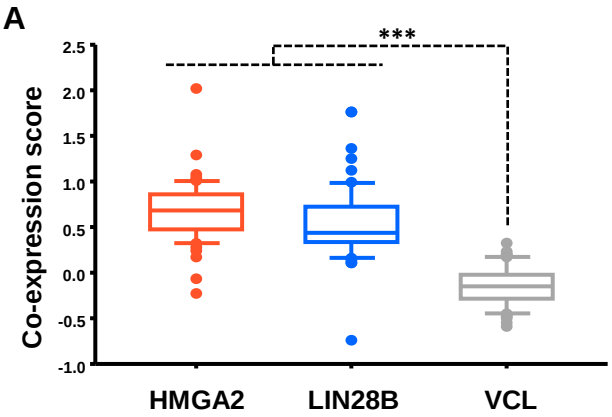

B

	Correlation in the CCLE (Array)		
	IGF2BP1 vs. HMGA2	IGF2BP1 vs. LIN28B	IGF2BP1 vs. VCL
Pearson r	0,2548	0,3167	-0,06975
p (two-tailed)	< 0,0001	< 0,0001	0,0347

	Correlation in ovarian cancer cell (RNA-Seq)		
	IGF2BP1 vs. HMGA2	IGF2BP1 vs. LIN28B	IGF2BP1 vs. VCL
Pearson r	0,7151	0,3276	0,1243
p (two-tailed)	< 0,0001	0,028	0,4159

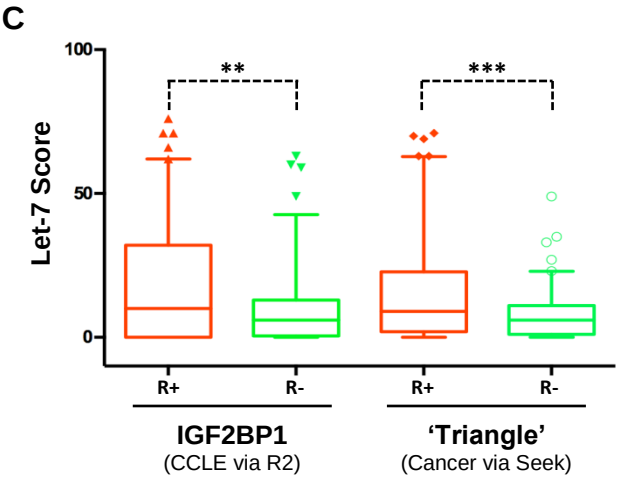

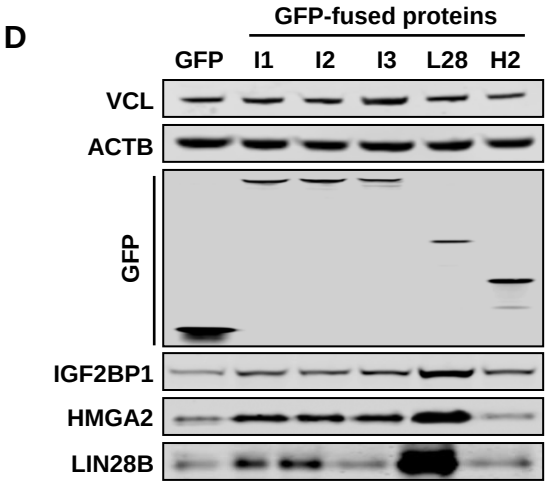

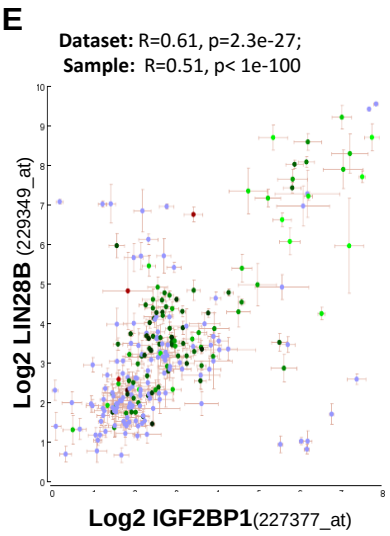

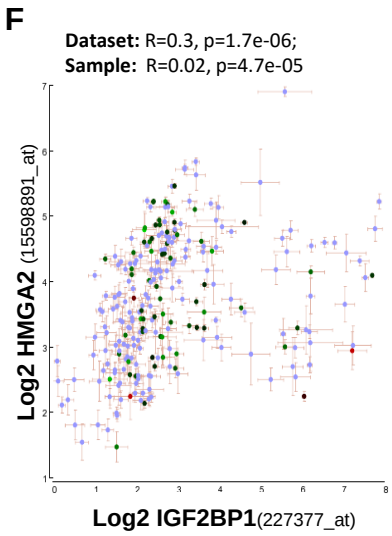

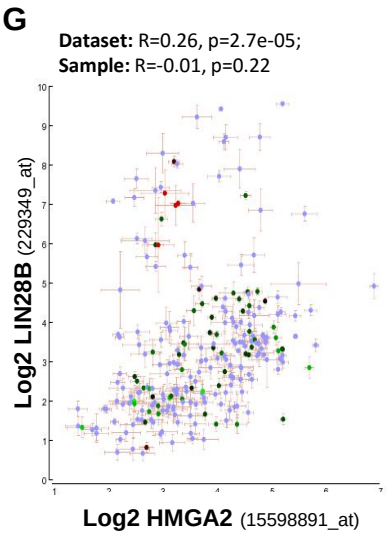

Supplemental Figure 9. Busch et al.

SUPPLEMENTAL MATERIAL AND METHODS

Protein purification, *in vitro* transcription and miTRAP

MBP-MS2BP was purified as previously described (65). *In vitro* transcription of RNA baits was performed on linearized DNA templates, essentially as described recently (32), using the following restriction enzymes: a) BclI: 2xMS2-control, IGF2BP1 3'UTRs; b) ApaI: LIN28B and HMGA2 3'UTRs. MiTRAP analyses were essentially performed as described recently (32). In variation, 40 pmol of each *in vitro* transcribed RNA bait or 2.5 pmol of MS2-control RNA were immobilized on MS2BP-MBP pre-coupled amylose resin for 1h. Cell-free extracts of $5x10^6$ ES-2 cells per condition were generated in BB (BB: 20mM Tris, pH 7.5, 150mM NaCl, 1.5mM MgCl2, 8.6% glycerol and 0.05% NP40) supplemented with protease inhibitor cocktail (1:200; Sigma Aldrich) and cleared by centrifugation. Cleared extracts were incubated with bait-coupled resin and supplements (11 mg/ml heparin, 1mM DTT and 400 U/ml RNAsin (Promega)) for 30 min. After four washing steps with heparin-supplemented BB, protein–RNA complexes were eluted twice in 150 µl BB supplemented with 15mM maltose. For RNA applications a phenol-chloroform extraction was performed. Integrity of bait RNAs was analyzed on agarose gels. Associated miRNAs were identified by small RNA-NGS analyses. For protein analysis, amylose resins were incubated with 25 µl of SDS-sample buffer supplemented with 10% beta-mercaptoethanol.

Deep sequencing analyses and databases

For miRNA sequencing, total RNA isolated by TRIZOL served as the template in the small RNA protocol using the TruSeqTM Small RNA Sample Prep Kit v2 (Illumina, San Diego, CA, USA) and size restriction between 140 and 165 nt, as described before (32). Library preparation and sequencing was carried out at the IZKF, University of Leipzig, Germany. A pool of 6 or 9 libraries was used for cluster generation per lane. For analysis of deep sequencing data all 50-bp reads from each lane were de-multiplexed and processed as described in (32). Alignment to mouse mature sequences of miRBase (5–8) was done with Bowtie2 aligner using miRBase v20 for DCR-/- knockout experiments (66). miTRAP experiments were aligned to human mature sequences of miRBase v19 using the Bowtie aligner (67). MiRNAs selectively down-regulated upon DCR-/- knockout or co-purified with the IGF2BP1-WT or MUT bait RNAs were identified using the edgeR software package of the R software environment for statistical computing (68). Deep sequencing data were normalized by the weighted trimmed mean of M-values method (TMM), which has proved to be suitable to normalize RNA-Seq data containing libraries with substantial distinct sizes (69). TMM-normalized miRNA counts, were used for differential expression or selective co-

purification of miRNAs based on Poisson exact testing (70). Enrichment or depletion of miRNAs was determined by a FDR < 0.05. For further details and the applied R script see Braun et al (32).

Publically available sequence alignment data files (.bam) of 45 ovarian cancer cell lines sequenced in context of the Cancer Cell Line Encyclopedia (CCLE) (59) were downloaded from the Cancer Genomics Hub (https://cghub.ucsc.edu/). Cell lines and data identifiers are summarized in Supplemental Table S3. These data were further processed according to an in-house developed RNA-Seq processing pipeline to ensure all the data were processed in the same way and to benefit from current gene annotations. Read sequences in FASTQ format were extracted from the provided alignment files using the bam2fastx program shipped with the TopHat2 (version 2.0.13) sequence alignment program (71). Illumina sequencing adapter sequences as well as low quality bases were trimmed off using the program cutadapt (version 1.6) (72). Subsequently, the remaining reads were mapped against the human genome (UCSC hg19 assembly (GRCh37)) using TopHat2 and sorted using samtools (version 1.1) (73). For ovarian cancer cell lines the number of reads spanning each single gene was determined using the program featureCounts (version 1.4.6) (74). Finally, raw count data were converted into FPKM (fragments per kilobase of transcript per million mapped reads) values using the R package edgeR (version 3.8.6) (68).

Accumulated read depth for 3'UTRs of IGF2BP1 mRNA isoforms was determined by analyzing the expression of IGF2BP1. Therefore BAM files of each sample were processed with BEDTools v2.23.0 (75) to extract the coverage of the IGF2BP1 3'UTR. Coverage of each nucleotide position was normalized to the coverage of the 3'UTR region (UCSC hg19 assembly (GRCh37)) and finally accumulated per sample type by calculating the median coverage. The complete analysis was performed in the R software environment for statistical computing.

Using multiMiR package (version 1.0.1) (76), the let-7 score for a gene was calculated as the weighed sum of let-7 family members (mature miRNA ID containing "hsa-let-7") putatively binding the gene's mRNA. Weights were defined as the number of databases predicting a specific interaction (0-8).

Where indicated publically available data were analyzed using the R2 platform (R2: Genomic Analysis and Visualization Platform, link: http://hgserver1.amc.nl/cgi-bin/r2/main.cgi) or SEEK platform (SEEK: Search-Based Exploration of Expression Compendium, link: http://seek.princeton.edu/index.jsp , (47)). Besides a global analyses over all datasets of the R2 database, the Cancer Cell Line Encyclopedia (CCLE) dataset consisting of 917 cancer-derived cell lines of different origin (59) as well as two primary cancer datasets (Ovarian Cancer – Pamula Pilat – 101 samples (60) ; Neuroblastoma – Versteeg – 88 samples (61)) were used.

Northern Blotting

Northern blot analyses for the detection of IGF2BP1 isoforms and GAPDH serving as loading control were performed according the Cold Spring Harbour Protocols (57). Briefly, 3 µg of polyadenylated RNA purified from total RNA with Oligotex (Qiagen) were incubated with glyoxol mix (60% DMSO, 20% glyoxal, , 80% glycerol, 2% ethidium bromide in BPTE puffer (100 mM PIPES, 300 mM Bis-Tris, 10 mM EDTA)) at 55°C for 1h and denatured for 10 min on ice. After the addition of loading buffer the RNA was separated on a 1% TAE-agarose-gel for 4h at 72V using GTG SeaKem Agarose (Lonza) and BPTE running buffer. RNA was transferred on nylon membrane using the WhatmanTM TurboblotterTM Transfer System (GE Healthcare) in 20xSSC overnight. Glyoxal reaction was stopped and membrane fixed by UV-crosslinking. ^{32}P-labeled DNA probes (indicated in Supplemental Table S6) were generated using the AmershamTM Megaprime DNA Labeling kit (GE Healthcare) and incubated overnight using the UltraHyb buffer (Ambio). After washing the Northern blot was analyzed by a phosphor imager (Strom 860; Molecular Dynamics) and quantified using the ImagingQuant 5.2 software.

Infrared Northern blotting of let-7a miRNA and 5S rRNA was essentially performed as described before (58). TRIZOL-purified total RNA (4 µg) was resolved on a 7% denaturing TBE-Urea-gel and subsequently blotted onto nylon membranes (Roche) using the tank blot system (Life Technologies). After crosslinking and pre-hybridization, with PerfectHyb Plus (Sigma-Aldrich) DY-782 label probes indicated in Supplemental Table S6 (MWG Biotech) were hybridized at 30°C for 2h and analyzed on an Odyssey Scanner (LI-COR).

Sucrose gradient centrifugation and RNA-Immunoprecipitation (RIP)

Cell were harvested, counted and lysed on ice in gradient buffer (10 mM Hepes pH7,0-7,2; 150mM KCl; 5mM $MgCl_2$) supplemented with 0.5% NP-40 and RNAsin for 10 minutes. OD_{260} of cleared lysates was determined to ensure equal loading of linear 5-20% sucrose gradients in gradient buffer without supplements. Gradients were centrifuged at 39,000 g for 2.5 h. Gradients were fractionated and UV profiles were recorded over 10 fractions (each ~1mL). The ribosomal pellet (RP) was derived by re-suspending residual precipitates. Protein and rRNA profiles of each fraction (1% v/v) were analyzed by Western blotting or ethidium bromide stained agarose gels, respectively. For mRNA and miRNA analyses, total RNA was isolated from 20% (v/v) of each fraction using Trizol purification. Let-7a levels were analyzed by Northern blotting (10% of each fraction). For mRNA analyses 25% of the recovered RNA (5% of input) was used for cDNA synthesis and analyzed by RT-PCR.

For RIP studies GFP-tagged proteins were precipitated from 0.5 mL of the mRNP fraction (fraction 5) using monoclonal GFP antibodies (see Table S7) immobilized to dyna beads (Thermofisher) in gradient buffer supplemented with RNAsin for 1 h. After three washing steps with gradient buffer (1 mL) protein-

RNA-complexes were eluted using gradient buffer supplemented with 1% SDS. 20% (v/v) of the eluates were used to monitor protein (co)-purification by Western blotting. For Western blotting 1% (v/v) total gradient input or 10% (v/v) of the mRNP input (fraction five) were used. RNA was extracted from 80% (v/v) of the total eluate using Trizol. The co-purification of mRNAs or the let-7a miRNA was determined by semi-quantitative PCR using 40 PCR cycles or Northern blotting, respectively. For inputs, RNA isolated from 10% (v/v) of total gradient input or 20% (v/v) of the mRNP fraction were used.

SUPPLEMENTAL FIGURE AND TABLE LEGENDS

Figure S1. IGF2BP expression in cancer-derived tumor cells and embryogenesis. (**A**) IGF2BP1 expression in indicated epithelial-like (green) tumor-derived cells versus HEK293A cells was determined by Western blotting. Note that 10-fold more protein (50 µg), compared to HEK293A controls (5µg), was loaded for epithelial-like cells. (**B**) The expression of the epithelial marker e-cadherin (CDH1) or the mesenchymal marker vimentin (VIM) was correlated (Pearson correlation) with IGF2BP1, IGF2BP2 or IGF2BP3 mRNA expression in the CCLE dataset via the R2 database. Correlation parameters are indicated. (**C** and **D**) IGF2BP1 protein and let-7a miRNA expression was analyzed in brain tissue of indicated mouse developmental stages and adult mouse brain tissue by Western (WB) and Northern (NB) blotting, respectively (C). GAPDH protein and 5S rRNA served as loading controls. Pearson correlation (indicated above graph) of normalized samples revealed a significant negative dependence of both factors during mouse brain development (D). (**E** and **F**) The Pearson correlation (paramters indicated above graphs, as determined by the R2 database) of IGF2BP2 (E) or IGF2BP3 (F) versus LIN28B mRNA expression in the CCLE dataset was analyzed via the R2 database. (**G-I**) Protein expression of IGF2BPs and LIN28B of 23 cancer-derived cell lines of different origins and HEK293A was analyzed by Western blotting (G) and quantified using VCL for normalization. Scatter blot of IGF2BP1 vs. LIN28B protein expression show a positive correlation of LIN28B and IGf2BP1 protein abundance (H). Pearson correlation parameters of IGF2BP protein abundance and LIN28B protein levels are summarized in (I). (**J**) LIN28B mRNA shows the strongest positive correlation to IGF2BP1 mRNA in a panel of 917 cancer-derived cell lines (CCLE dataset, R2 database) as indicated by rank position 1. Correlation parameters are shown. “Present” indicates the number of cell lines with reliable signal intensities based on Affymetrix u133p2.0 chip and MAS5 normalization.

Figure S2. Pearson correlation of long and total IGF2BP1 mRNA variants in tumor-derived cell lines and primary ovarian cancer. (**A, C**) The schematic (top panel in A) indicates the full length IGF2BP1 transcript with APA sites (black triangles) and the positions of IGF2BP1 identifiers (black bars and boxes) used on Affymetrix u133p2.0 gene chips. Pearson correlation (parameters indicated in graphs) reveals a significant and positive correlation of both IGF2BP1-directed identifiers in the CCLE dataset comprising expression data of 917 cancer-derived cell lines (A) and the combined data for both identifiers determined in two independent ovarian cancer data sets described in Figure 2B (C). All expression data were normalized by Mas5 and obtained from the R2 database. (**B**) The schematic (top panel) indicates the last three exons of the *IGF2BP1* gene locus used to determine median read coverage of total versus

long IGF2BP1 mRNAs as determined by RNA-sequencing. APA sites (black triangle) in the 3'UTR (solid black line), introns (dashed black lines) and exons (black boxes) are indicated. Pearson correlation was used to determine the median sequence coverages over 45 ovarian cancer-derived cell lines analyzed by RNA-sequencing in the CCLE, as described in Figure 2A. Note that long and total transcript abundance is significantly and positively correlated supporting the microarray-based analyses (see A, C). (**D**) The schematic (top panel) shows the longest IGF2BP1 mRNA with APA sites (black triangles) and PCR amplicons used to determine the expression of total versus long transcripts by RT-PCR (also refer to Figure 2C, D). The Pearson correlation (parameters in graph) of long versus total IGF2BP1 mRNA abundance, as determined by RT-qPCR in 29 ovarian carcinoma-derived samples described in Figure 2C, reveals a significant and positive correlation. Taken together the analyses indicate that the long IGF2BP1 transcripts become upregulated along with increased IGF2BP1 mRNA synthesis in cancer-derived cells and primary ovarian cancer. This suggests that the enhancement of APA is negligible for increased IGF2BP1 expression in ovarian cancer.

Figure S3. IGF2BP1 3'UTR mainly associates with let-7 miRNAs. (**A**) The fold change abundance of IGF2BP paralogue-encoding mRNAs in DCR1 (-/-) MEFs was determined by RT-qPCR relative to wild type MEFs using TUBA4A mRNA levels for normalization. Note that GAPDH mRNA levels remain essentially unchanged whereas mRNAs encoding IGF2BPs are upregulated. (**B**) MiRNA abundance in DCR1(-/-) MEFs was determined relative to wild type MEFs by miRNA sequencing. The fold change of miRNA levels was determined by a Poisson exact test upon TMM-normalization of miRNA logCPMs. Three independent libraries were analyzed per condition. Notably, the increase of miRNAs observed in DCR1 (-/-) MEFs might be due to normalization of the data by the TMM (Trimmed mean of M-value) since library sizes were ~5-fold lower in DCR1 (-/-) derived samples. Moreover, DCR1-independent miRNAs as well as mRNA or ncRNA degradation products are reported among these putatively up-regulated small RNAs (77,78). (**C**) The activity of luciferase reporters comprising the longest wild type (WT), let-7 MRE-mutated (MUT) 3'UTRs of IGF2BP1 or only the pmiR-Glo encoded MCS (MCS) was determined in wild type or DCR1 (-/-) MEFs. Error bars indicate the s.d. of at least three independent analyses of Renilla-normalized Firefly activity ratios (DCR1 (-/-) versus wild type MEFs). Statistical significance was determined by (two-sided) Student's t-test: ** $P<0.005$; *** $P<0.0005$. Note that the inactivation of let-7 MREs does not abolish elevated reporter activity in DCR1 (-/-) MEFs suggesting let-7 independent regulation of the MUT-reporter. (**D**) The pie chart shows the percentage of let-7 miRNA counts (green) relative to the total count of miRNAs selectively co-purified with the wild type IGF2BP1 3'UTR in miTRAP analyses (see Figure

3E). The s.d. of miRNA counts was determined in three independent miTRAP studies. (**E**) Putative MREs for the indicated miRNAs in the longest IGF2BP1 3'UTR were determined by miRANDA or RNA-hybrid, essentially as previously described (32). MREs overlapping with validated let-7 MREs are indicated in red. The position of the 5'-nt of the putative MRE in the longest IGF2BP1 3'UTR is indicated.

Figure S4. Inhibition of let-7 activity in ovarian cancer and HCC cell lines. (**A**) Sequence homology of the human let-7 miRNA family with seed sequence (grey shadow) and nucleotide variations (red). (**B**) The expression of indicated proteins and let-7a was analyzed by Western and Northern blotting in four ovarian cancer-derived cells (Cov318, ES-2, OVCAR-3 and SK-OV-3) and HCC-derived Huh7 cells. VCL, TUBA4A, ACTB and 5S served as loading controls. Let-7a expression inversely correlated with the expression of triangle factors and was barely or non-detectable in Cov318 or Huh7 cells, respectively. (**C**) Renilla-normalized activities of let-7a and let-7i Firefly anti-sense luciferase reporters confirm distinct let-7 abundance (see B) in the respective cancer-derived cell lines. Note that no or marginal repression of both reporters was observed in Huh7 or Cov318 cells. (**D**) Expression of the long vs. total IGF2BP1 transcript abundance in cancer-derived cells was determined by RT-qPCR with using HEK293A cells as a reference (also see Figure 1D). The long IGF2BP1 mRNAs provide ~50-60 % of total IGF2BP1-encoding transcripts in the analyzed tumor-derived cell lines, as also observed in Figure 1D. (**E**, **F**) Let-7 activity was impaired by let-7 directed decoys (also see Figure 4) upon lentiviral transduction in indicated cell lines. Let-7 activity was determined by let-7a and let-7i anti-sense reporter assays (E), as described in (C). IGF2BP1, LIN28B and HMGA2 protein expression was determined by quantitative Western blotting in indicated cells transduced with control (C) or let-7 directed decoys. GAPDH and TUBA4A were used for normalization to determine protein ratios (let-7 vs. control decoy) in three independent analyses, as indicated below lanes. Note that different amounts of total protein were loaded for distinct cell lines (Cov318, 5µg; OVCAR-3 and SK-OV-3, 30 µg) due to the severe difference in protein abundance (see B). In SK-OV-3, IGF2BP1 and LIN28B levels were not detectable (n.d.), presumably due to transcriptional silencing or exceedingly low mRNA synthesis. Error bars indicate the s.d. of at least three independent analyses.

Figure S5. IGF2BP1, LIN28B and HMGA2 form a self-promoting triangle. (**A**) Schematics of PAR-CLIP hits (red), as determined by CLIPdb (link: http://lulab.life.tsinghua.edu.cn/clipdb/) according to (40) for IGF2BP1-associated transcripts, as well as let-7 MREs (blue) determined by targetscan database according to (4,6) in IGF2BP1, LIN28B or HMGA2. (**B**) Western blotting of indicated proteins co-purified with the wild type (WT) or let-7 MRE-mutated (MUT) 3'UTRs of IGF2BP1, LIN28B or HMGA2 (top to bottom) from ES-2 cells in miTRAP analyses (see Figure 3). Note that the co-purification of AGO2 is

reduced for the MUT bait RNAs whereas IGF2BP1-association appears unaffected. Representative Western blots of three analyses are shown. (**C**) The abundance of indicated proteins was analyzed by Western blotting in ES-2 cell populations in which IGF2BP1 expression was essentially abolished by CRISPR/CAS9 (IGF2BP1-KO) or which had been transduced with GFP-encoding vectors (C). Where indicated (bottom) IGF2BP1-KO cells were transduced with lentiviral vectors encoding the indicated GFP-tagged proteins. The fold change of protein abundance (indicated above lanes) was determined relative to GFP-transduced cells. Errors indicate the s.d. determined in three independent analyses. VCL served as loading control. Error bars indicate the s.d. of at least three independent analyses. Statistical significance was determined by a (two-sided) Student's t-test: * P<0.05; ** P<0.005.

Figure S6. IGF2BP1-LIN28B-HMGA2 form a self-promoting triangle antagonized by let-7 miRNAs. (**A**) GFP-fused IGF2BP1 was overexpressed in cell lines with let-7 levels barely (Cov318) or non-detectable (Huh7) by Northern blotting or miRNA anti-sense reporters (see Figure S4B, C). Cells stably expressing GFP or the RNA-binding deficient mutant of IGF2BP1 (IGF2BP1mut) served as controls. The abundance of indicated proteins was analyzed by semi-quantitative Western blotting. Altered expression of triangle factor proteins (indicated above lanes) in GFP-IGF2BP1 or GFP-IGF2BP1mut expressing cells was determined relative to GFP using VCL and ACTB for normalization in three independent analyses. Notably, in cell lines with negligible let-7 and exceedingly high IGF2BP1 levels, enhanced expression of triangle factors is not or barely observed. This suggests that the shielding of IGF2BP1 target mRNAs from let-7 attack is negligible in the absence (Huh7) or at exceedingly low (Cov318) let7 abundance. (**B, C**) The expression of indicated proteins (B) or corresponding mRNAs (C) was analyzed by Western blotting or RT-qPCR in ES-2 cells stably transduced with indicated GFP-tagged proteins. The fold change (C) of mRNA (grey) or protein (black) abundance in ES-2 cells stably expressing the indicated GFP-tagged proteins was determined relative to GFP-transduced control cells. Error bars indicate the s.d. of at least three independent analyses. Statistical significance was determined by a (two-sided) Student's t-test: * P<0.05; ** P<0.005.

Figure S7. The HMGA2-LIN28B-IGF2BP1 triangle antagonizes the let-7 directed repression of tumor cell growth and self-renewal without affecting apoptosis. (**A**) The number of viable ES-2 cells transduced with decoys and transfected with siRNA pools as indicated was analyzed by flow cytometry (FC) upon PI-labeling. The change of cell numbers is shown relative to non-transfected ES-2 cells transduced with control decoys (TuD-C), essentially as depicted in Figure 7C. (**B**) The percentage of dead ES-2 cells transduced and transfected as in (A) was determined by PI-labeling in FC-studies (see A). Note that cell death appears essentially unaffected suggesting that apoptosis was not increased upon triangle factor

depletion. (**C**) The volume of spheroids formed by ES-2 cells transduced and transfected as indicated (also see Figure 7B and C) was determined by spheroid diameters determined by light microscopy (see Figure 6B) assuming a perfectly spherical morphology using the formula ($V=1/6*\pi*d^3$). Error bars indicate s.d. of at least three independent analyses. Statistical significance was determined by a (two-sided) Student's t-test: * $P<0.05$; ** $P<0.005$; *** $P<0.0005$, ns $P\geq0.05$.

Figure S8. The LIN28B-IGF2BP1 axis antagonizes let-7 directed repression of 2D tumor cell migration. (**A**) The morphology of ES-2 cells transduced with decoys and transfected with triangle factor directed or control siRNA pools as indicated was analyzed by F-actin labeling using phalloidin, immunostaining of β-catenin (CTNNB1) and staining of nuclei by DAPI. Representative images are shown. Enlargements of boxed regions (upper panel) are shown in the lower panel. Bars, 25 µm. Note that the recruitment of CTNNB1 to cell-cell contacts appears increased upon the depletion of IGF2BP1 and LIN28B but essentially unchanged by the knockdown of HMGA2. (**B** and **C**) The migration of ES-2 cells transduced with decoys and transfected siRNA pools as indicated was analyzed on 2D collagen matrices by time lapse live cell microscopy. The migratory tracks of individual cells (B) served for determining the mean speed of 2D cell migration. The mean speed determined for individual cells (n>50, analyzed cells) is depicted by box plots (C). Statistical significance was determined by a (two-sided) Student's t-test: * $P<0.05$; *** $P<0.0005$; ns $P\geq0.05$.

Figure S9. The HMGA2-LIN28B-IGF2BP axis is active in a broad range of cancers. (**A**) The co-expression of IGF2BP1 with HMGA2, LIN28B and VCL was analyzed via the SEEK database. The co-expression scores determined for all tissue-specific cancer and non-cancer data sets provided via SEEK are depicted as box plots. VCL served as the control for none significantly associated expression. Significance was determined by a (two-tailed) Student's t-test: ***, $P<0.0005$. (**B**) The expression of IGF2BP1 was correlated with the abundance of HMGA2, LIN28B or VCL mRNAs in the complete CCLE microarray (Array) or with the RNA-sequencing data set (RNA-Seq) comprising data of all ovarian cancer cells (45) analyzed in the CCLE. Pearson correlation parameters are indicated. (**C**) The let-7 targeting scores of the top 100 genes positively (red, R+) or negatively (green, R-) associated with IGF2BP1 in the CCLE dataset of the R2 database or with HMGA2-LIN28B-IGF2BP1 (Triangle) in all cancer data sets comprised in the SEEK database were determined via the multiMiR R package. Targeting scores are depicted by box plots. Statistical significance was analyzed by (two-sided) Student's t-test: **, $P<0.05$; ***, $P<0.0005$. (**D**) The expression of indicated proteins was determined in ES-2 cells stably transduced with GFP, GFP-tagged IGF2BPs (I1-I3), GFP-LIN28B (L28) or GFP-HMGA2 by Western blotting. VCL and ACTB served as loading

controls. Note that all IGF2BPs enhance the expression of HMGA2 and endogenous IGF2BP1. Forced expression of IGF2BP1 and IGF2BP2 also enhances the abundance of LIN28B. GFP-LIN28B resulted in the strongest upregulation of IGF2BP1, HMGA2 and LIN28B protein levels. GFP-HMGA2 only modestly enhanced the expression of IGF2BP1. (**E-G**) The correlation of IGF2BP1 and LIN28B (A), IGF2BP1 and HMGA2 (B) or HMGA2 and LIN28B (C) mRNA expression was analyzed by the 2D gene expression overview cross data set analysis tool of the R2 database. The correlation of expression is shown across 250 distinct cancer data sets. Significant positive (green), negative (red) or non-significant (blue) correlation of gene expression in individual samples is indicated. Pearson correlation data for the cross-data set analysis (dataset) or within analyzed samples (sample) is indicated in graphs.

Table S1. MiRNA expression profile of DCR1 (-/-) vs. DCR1-WT MEFs. MiRNA expression of Dicer1-KO (DCR1 -/-) vs. Dicer1 WT-MEFs was analyzed by small RNA sequencing. Raw counts, CPMs determined by TMM normalization, fold changes (logFC), average expression (av.logCPM) and p-values are shown. Differential expression (-1, green, down-regulated; 1, red, up-regulated or 0, yellow unchanged) was determined by a Poisson exact test using a p-value threshold of 0.05. MiRNAs that could be derived by non-specific degradation of mRNAs or ncRNAs are labeled in red (77).

Table S2. MiTRAP analyses of IGF2BP1-3'UTRs. MiTRAP experiments using the wild type (WT) or let-7 MRE-mutated (MUT) 3'UTRs of IGF2BP1 vs. MS2 control as baits were analyzed by small RNA sequencing (see Figure 3). Raw counts, CPMs determined by TMM normalization, fold changes (logFC), average expression (av.logCPM), p-values and the average CPMs of input fractions (av-Input CPM) are shown as table. The enrichment score (E-score) was determined as previously described (32).

Table S3. Ovarian cancer cell lines included in CCLE data sets. Ovarian cancer cell lines analyzed in the CCLE by RNA-sequencing and microarray analyses are shown. Identifiers of NGS (Cancer Genome Hub) are indicated.

Table S4. Plasmids and cloning strategies. Plasmids used in this study are shown. Cloning strategies including vectors, PCR primers and restriction sites are indicated. Constructs obtained from Addgene or described in previous studies are indicated.

Table S5. Real-time PCR oligonucleotides. PCR primers and sequences used in this study are shown.

Table S6. Northern blotting probes. Probes, sequences and fluorophores used for probe labeling labels are indicated. Probes without fluorescence tags were labeled with ^{32}P-αdCTP.

Table S7. Primary antibodies. Primary antibodies used in this study are indicated along with vendor and item number information.

Table S8. siRNAs and miRNAs. Synthetic siRNA combined to siRNA pools as indicated and synthetic miRNAs as well as sequences are shown.